Proceedings of the ASME 2010 3rd Joint US-European Fluids Engineering Summer Meeting and 8th International Conference on Nanochannels, Microchannels, and Minichannels
FEDSM-ICNMM2010
August 1-5, 2010, Montreal, Canada

FEDSM-ICNMM2010-31122

DNS STUDY OF TRANSITIONAL CHANNEL FLOW ACCOMPANIED BY TURBULENT-STRIPE STRUCTURES

Shizuma Kaneko
Dept. of Mechanical Engineering
Tokyo University of Science
Noda-shi, Chiba 278-8510, Japan
Email: j7509614@ed.noda.tus.ac.jp

Takahiro Tsukahara*
Dept. of Mechanical Engineering
Tokyo University of Science
Noda-shi, Chiba 278-8510, Japan
Email: tsuka@rs.noda.tus.ac.jp

Yasuo Kawaguchi
Dept. of Mechanical Engineering
Tokyo University of Science
Noda-shi, Chiba 278-8510, Japan
Email: yasuo@rs.noda.tus.ac.jp

ABSTRACT

A regular pattern of turbulent and quasi-laminar fluid motion is known to appear in plane Poiseuille flow near the lowest Reynolds number for which turbulence can be sustained. We focused on this transitional structure called the turbulent stripe and investigated its energy transport process, using a direct numerical simulation. We obtained the budget for Reynolds stresses including $v'w'$ and $w'u'$. The spatial outline of the energy transport with respect to the turbulent stripe is proposed. The turbulent energy is produced in both the turbulent region and the quasi-laminar region, and the energy transfer between these two regions is found to be small.

INTRODUCTION

In the present work, we consider a plane Poiseuille flow. This flow is characterized by a single non-dimensional parameter, i.e., the Reynolds number, defined as $Re_\tau = u_\tau \delta/\nu$, where δ is the half gap between the plates, u_τ is the friction velocity, and ν is the kinematic viscosity of fluid. Although a turbulent channel flow, as one of the canonical wall turbulence, has been studied in a wide-range of the Reynolds number by a number of researchers, both computational and experimental studies on the subcritical transitional channel flow are few in number and rarely demonstrated spatially intermittent turbulence in the channel flow.

The intermittent turbulent structure, that emerges in various sheared flows at transitional Reynolds numbers, has been investigated. Recently, the turbulent structure similar to the puff in a transitional pipe flow was found in a transitional channel flow by Tsukahara et al. [1–4] through a direct numerical simulation (DNS). This structure is called the "turbulent-stripe" structure (TSS), consisting of a turbulent region and a quasi-laminar region, each with a stripe pattern. Further observations of the TSS as well as that in a plane Couette flow have been reported in these years [6–8]. Barkley & Tuckerman [6] carried out simulations of the turbulent Couette flow in a computational domain, which was inclined with respect to the mean flow direction. They revealed that once the Reynolds number, based on the channel width and the wall velocity, decreased from 500 to 350, turbulent and quasi-laminar regions spontaneously appeared and remained in coexistence. In their study, the turbulent statistics were spatially averaged along the stripe pattern, and the secondary flows were investigated in detail. The experiments [9, 10] of Taylor-Couette flow first showed this kind of intermittent turbulent structure called the spiral turbulence, which was laminar and turbulent regions coexist in a spiral shape. In our previous studies, we performed the direct numerical simulations of a turbulent Poiseuille flow using an extremely large computational domain and found that, in the low Reynolds numbers of $Re_\tau = 56$–80, the Poiseuille flow contained several localized turbulent bands, as similar to those observed in the plane Couette and the Taylor-Couette flows. In the flow, the quasi-laminar and turbulent regions was found to

*Address all correspondence to this author.

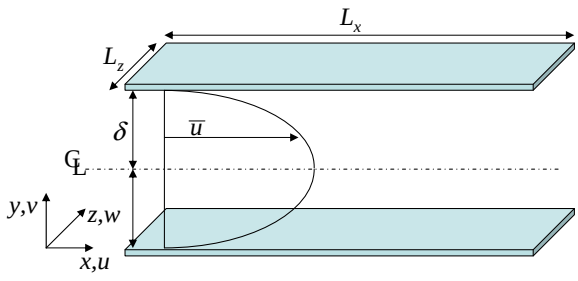

Figure 1. Flow configuration and coordinate system.

form the stripe pattern, which inclined at 24° against the streamwise direction and maintains itself over a long time. However, the self-sustaining mechanism of the TSS has not been fully understood.

In the present work, we performed DNS of a turbulent Poiseuille flow at a low Reynolds number. We investigated the self-sustaining mechanism of the TSS by analyzing energy budgets of Reynolds stresses. In addition, we applied the rheoscopic-fluid visualization technique [13] to visualize the flow field and compared with experimental observations [14]. A rheoscopic-fluid is one that allows the viewer to see the features of the flow directly, as explained in a later section.

DNS DETAILS

The objective flow field is a channel flow, as given in Fig. 1. Throughout this paper, x (u), y (v) and z (w) denote the streamwise, wall-normal and spanwise directions (velocities), respectively. The mean flow is driven by the uniform pressure gradient. It is assumed to be fully developed in the streamwise and spanwise directions. Periodic boundary condition is imposed in the horizontal directions, and non-slip condition is applied on the walls. The fundamental equations are the continuity and the Navier-Stokes equations:

$$\frac{\partial u_i^+}{\partial x_i^*} = 0, \tag{1}$$

$$\frac{\partial u_i^+}{\partial t^*} + u_j^+ \frac{\partial u_i^+}{\partial x_j^*} = -\frac{\partial p^+}{\partial x_i^*} + \frac{1}{Re}\frac{\partial}{\partial x_j^*}\left(\frac{\partial u_i^+}{\partial x_j^*}\right) + \delta_{1i}. \tag{2}$$

where δ_{1i} corresponds to the mean pressure gradient, and quantities with the superscript of $^+$ indicate those normalized by the wall variables. They are normalized by the characteristic velocity u_τ from the mean pressure gradient, the channel half width δ, the fluid viscosity ρ, and the kinematic viscosity ν. For the spatial discretization, the finite difference method is adopted. Further details of the method can be found in our previous reports [1, 2]. Uniform grid mesh is used in the streamwise and spanwise directions, and non-uniform mesh in the wall-normal direction. At $Re_\tau = 80$, the wall-normal grid spacings are $\Delta y^+ = 0.22$–3.59, which correspond to 0.13η–1.25η (η is referred to as a local Kolmogorov scale). These grid spacings are finer than ones used by Abe *et al.* [5], whose grid resolutions were approximately equal to 0.3η–1.6η. A fully-developed flow field at a moderate Reynolds number was used as the initial condition. Note that various statistical data and visualized fields have been obtained after the flow field reached statistical-steady state. As for two-dimensional contours shown after, quasi-mean velocities and budgets of Reynolds shear stresses are averaged for a time of $150\delta/u_\tau$ (i.e., $9600\nu/u_\tau^2$; 40 wash-out times). We employed a computational domain of $L_x \times L_y \times L_z = 51.2\delta \times 2\delta \times 25.6\delta$ with $1024 \times 96 \times 512$ grids. This size of the domain can capture a single localized turbulent region, i.e., a single turbulent-laminar band, in order to discuss the mechanism through which the TSS sustains itself.

RESULTS AND DISCUSSION

In the present study, we confirmed the appearance of a TSS at low Reynolds number of $Re_\tau = 80$. In the following sections, we shall recapitulate the rheoscopic-fluid visualization technique to extract TSS in the flow field and compare them with those observed by experimental study. After that, some details are presented to show mechanisms of the TSS through analysis of the budget of the transport equations for Reynolds stresses. Finally we will describe an outline of the spatial transport of turbulent kinetic energy concerning the structure.

DNS visualization

Figure 2(a) displays a snapshot of the flow with iso-surfaces of the streamwise velocity fluctuation at $Re_\tau = 80$ ($Re_m = 2400$), in which positive and negative fluctuations clearly exhibit a snapshot of large-scale oblique pattern. To make a comparison with experimental flow visualization using flake particles, the fluid is visualized as a rheoscopic fluid and by volume rendering. It is known that a flake particle follows a direction of a local shear layer so that the normal vector of a flake $\mathbf{n}$ is formulated by the following equation,

$$\mathbf{n} = 2\mathrm{D}\mathbf{u}\hat{\mathbf{u}} - \left(\hat{\mathbf{u}}^{\mathrm{T}}\mathrm{D}\mathbf{u}\hat{\mathbf{u}}\right)\hat{\mathbf{u}} \tag{3}$$

where $\mathbf{u}$ is the fluid velocity, $\hat{\mathbf{u}}$ is the unit vector of $\mathbf{u}$, and $\mathrm{D}\mathbf{u}$ is the strain-rate tensor. Angles of the light-source and observation directions are referred as θ and ϕ, respectively. From the relationship between three vectors of $\mathbf{n}$, θ, and ϕ, the intensity of reflected light can be evaluated.

Figures 2(c) and 2(d) show the present results of volume-rendering visualization, and Fig. 2(b) shows an experimental ob-

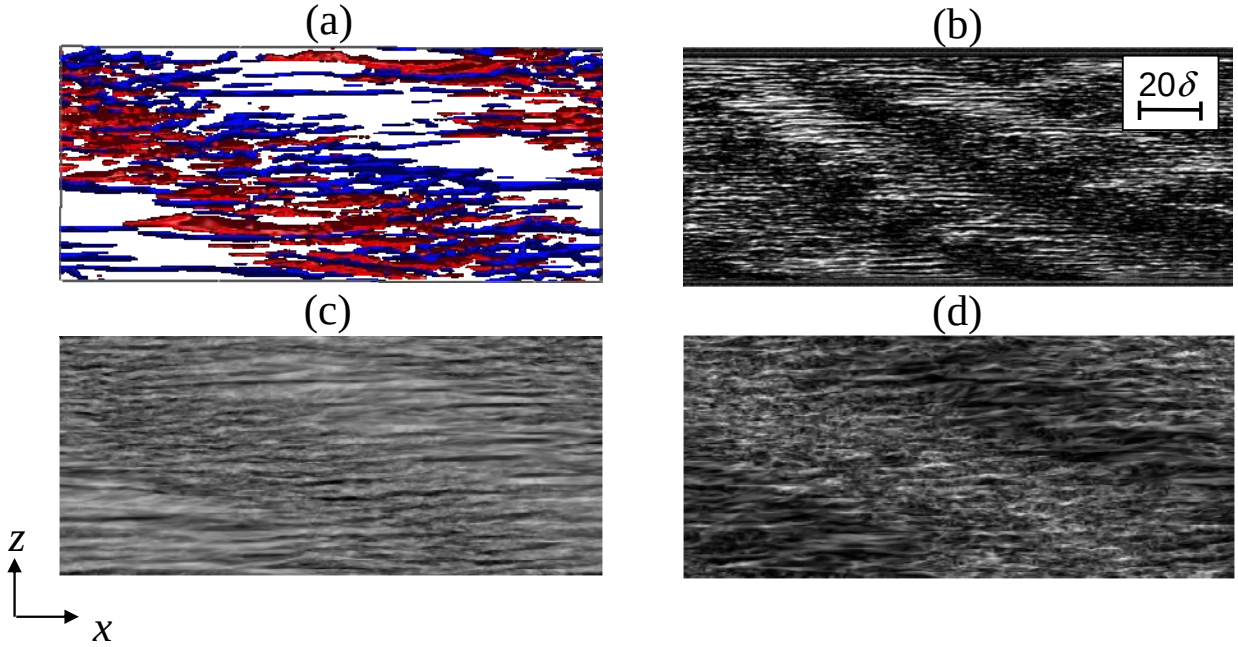

Figure 2. Comparison of visualization results on turbulent stripe. (a) Iso-surface of fluctuation velocity, red is $u'^{+} > 2$; blue is $u'^{+} < -2$. (b) Experimental visualization. (c) Numerical rheoscopic fluid visualization ($\theta = -45$ degree and $\phi = 90$ degree). (d) Numerical rheoscopic fluid visualization ($\theta = 45$ degree and $\phi = 90$ degree). The visualized areas are of $51.2\delta \times 25.6\delta$ in (a,c,d) and of $164\delta \times 82\delta$ in (b).

servation by Hashimoto *et al.* [14]. Figure 2(c) is given for $\theta = -45^{\circ}$ and $\phi = 90^{\circ}$—note that an angle of 0° corresponds to the z axis in the z-y plane—, while Fig. 2(d) is for $\theta = 45^{\circ}$ and $\phi = 90^{\circ}$. In the present results using a rheoscopic fluid in the same experimental condition of the light source and the camera angle, the turbulent region is found to be bright and the quasi-laminar region is relatively dark. From this method, fine-scale vortices can be observed clearly in the localized turbulent region. On the other hand, large-scale streaks are found in the quasi-laminar region, and they are elongated in the streamwise direction, revealing the existence of longitudinal vortices there: see Fig. 2 (b). Although the present method is useful as an index by which the turbulent region and the quasi-laminar region are distinguished, the relationship between the brightness and the flow state (laminar or turbulent) in the numerical visualization is inconsistent with the experimental results. This is because the large-scale streaks in the quasi-laminar region are dominant, since the reflected light intensities from fine-scale eddies are rather weak in experimental observation.

Ensemble-averaged flow field

The oblique pattern of TSS captured in the present DNS is confined by the periodic boundaries in both streamwise and spanwise directions, and parallel to a diagonal of the domain, as given in Fig. 2(a). As can be seen from the figure, the TSS is elongated across the domain in its diagonal direction. Let us define z' as the coordinate parallel to the diagonal line. A spatial-averaged value in the z' direction and a fluctuation from the mean value are defined as:

$$\overline{u_i}^{z'}(x,y) = \frac{1}{T}\frac{1}{\sqrt{L_x^2+L_z^2}}\iint u_i(x+t\cdot u_m, y, z', t)dz'dt,$$
$$u_i'(x,y,z) = u_i(x,y,z) - \overline{u_i}^{z'}(x,y), \tag{4}$$

while the usual averaging in x-z plane (z'-averaging) is;

$$\overline{u_i}(y) = \frac{1}{T}\frac{1}{L_x\cdot L_z}\iiint u_i(x,y,z,t)dxdzdt,$$
$$u_i''(x,y,z) = u_i(x,y,z) - \overline{u_i}(y). \tag{5}$$

By assuming homogeneity of the TSS in the z'-direction and its propagation speed equal to the bulk mean velocity u_m, the ensemble-averaged velocity fields with respect to the TSS are obtained. This z'-averaging can remove the large-scale fluctuation (due to the TSS) from the fluctuating component.

The mean-velocity distributions in the x-y plane are shown in Figs. 3(a), (b) and (c), which represent the streamwise, wall-normal and spanwise components, respectively. Moreover, the flow field can be classified to four regions as the following:

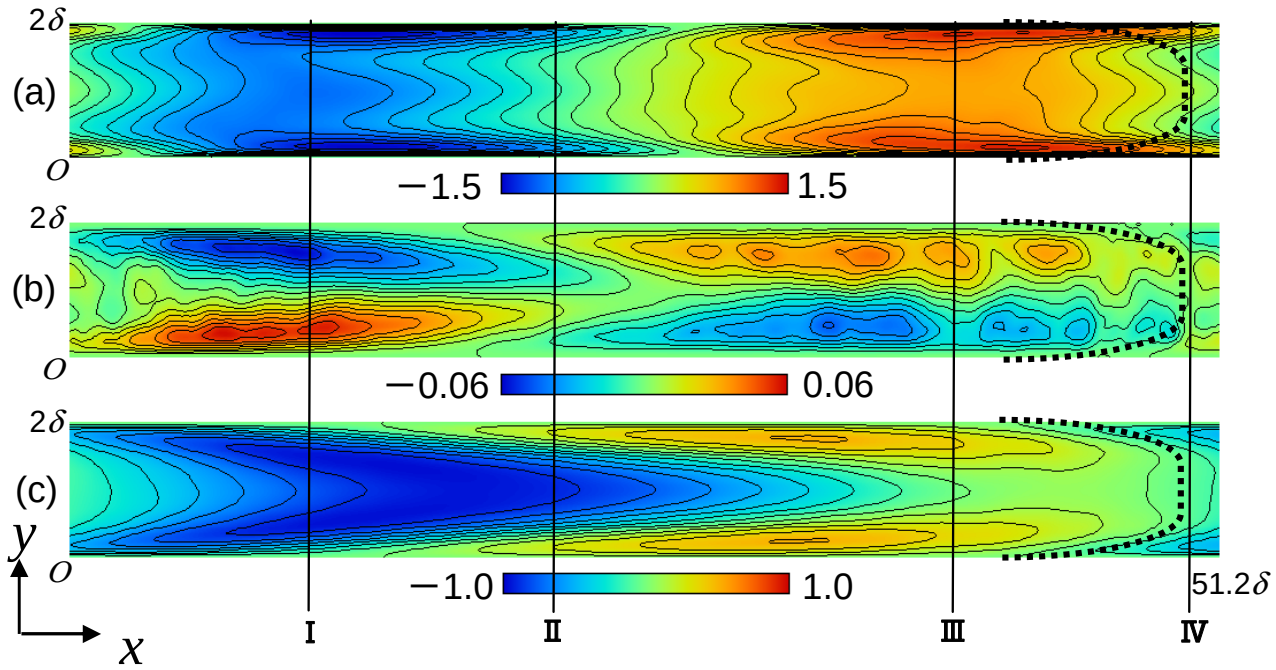

Figure 3. Quasi-mean flow in an (x-y) frame of reference moving with the turbulent stripe: (a) quasi-mean streamwise velocity, (b) quasi-mean wall-normal wise velocity, (c) quasi-mean spanwise velocity.

the upstream high-momentum (around the vertical-line III), the downstream low-momentum region (I), a strong-turbulent zone (IV), and a weak-turbulent zone (II) appear. The dotted line designates the edge of the high-speed fluid region. It is found that the large-scale regions of high- and low-speed fluctuations appear occupying the whole width in the wall-normal direction. The intrusion of high-speed fluid is clearly observed in Fig. 3(a), where the high-speed fluid indicated in red are squeezed into the upstream interface at the core region, and an internal strong shear layer ($\partial u'/\partial y$) is generated there. In the near-wall region, however, the high-speed fluids collide with the low-speed fluids ahead, which generated the flow toward channel center. The quasi-mean wall-normal velocity, shown in Fig. 3(b), is as large as 0.06 around the turbulent region, while the mean wall-normal velocity in the fully turbulent channel flow should be zero. As shown in Fig. 3(c), at around the upstream interface, a significant negative spanwise flow is generated at the channel center, while the positive spanwise flow is generated in the near-wall region at around the downstream interface.

Budgets of reynolds stress

Each budget term of the transport equation for Reynolds stress $\overline{u_i'^+ u_j'^+}$, in the fully-developed channel flow field, can be expressed as

$$\frac{\mathrm{D}}{\mathrm{D}t}\left(\overline{u_i'^+ u_j'^+}\right) = P_{ij} + T_{ij} + D_{ij} + \Pi_{ij} - \varepsilon_{ij}, \tag{6}$$

where the terms on the right-hand side are described as follows:

$$\text{Production}: P_{ij} = -\left(\overline{u_i'^+ u_k'^+}\frac{\partial \overline{u_j^+}}{\partial u_k^+} + \overline{u_j'^+ u_k'^+}\frac{\partial \overline{u_i^+}}{\partial u_k^+}\right) \tag{7}$$

$$\text{Turbulent Diffusion}: T_{ij} = -\frac{\partial}{\partial u_k^+}\left(\overline{u_i'^+ u_j'^+ u_k'^+}\right) \tag{8}$$

$$\text{Molecular Diffusion}: D_{ij} = \frac{\partial^2}{\partial u_k^{+2}}\left(\overline{u_i'^+ u_j'^+}\right) \tag{9}$$

$$\text{VPG}: \Pi_{ij} = -\left(\overline{u_j'^+ \frac{\partial p'^+}{\partial x_i^+}} + \overline{u_i'^+ \frac{\partial p'^+}{\partial x_j^+}}\right) \tag{10}$$

$$\text{Dissipation rate}: \varepsilon_{ij} = 2\overline{\left(\frac{\partial u_i'^+}{\partial x_k^+}\right)\left(\frac{\partial u_j'^+}{\partial x_k^+}\right)} \tag{11}$$

Here, the VPG term denotes the velocity pressure-gradient correlation term. In Fig. 4, we plotted the budget of the Reynolds stress $\overline{u'u'}$, as a function of the dimensionless wall distance y^+,

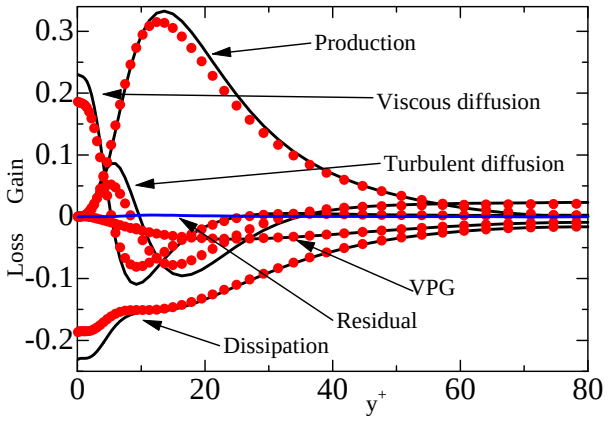

Figure 4. Budget of Reynolds stress $u'u'$: line, averaging in x-z plane;

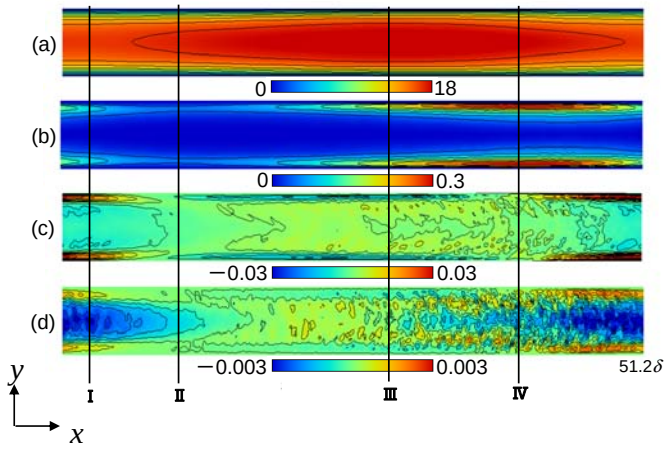

Figure 5. Quasi-mean flow in an (x-y) frame of reference moving with the turbulent stripe: (a) quasi-mean streamwise velocity, (b) turbulent kinetic energy, (c,d) advection term of budgets for Reynolds stresses $u'u'$ and $v'v'$.

for the result calculated by the z'-direction averaging and those by the x-z plane averaging. The budget of Reynolds stresses for $\overline{v'v'}$ and $\overline{w'w'}$ (not shown here) did not show a significant discrepancy between the two averaging, but the budget of $\overline{u'u'}$ did. The production term is found to be decreased in the case of z'-averaging, due to canceling the large fluctuation of the TSS. The dissipation and the diffusion terms in the near-wall region are also decreased. However, the VPG term does not depend on the averaging procedure, and thereby the budgets both for $v'v'$ and $w'w'$ are not difference between the two averaging.

Figure 5(a) reveals that large-scale regions of the high- or low-speed fluctuation appear occupying the whole width in the

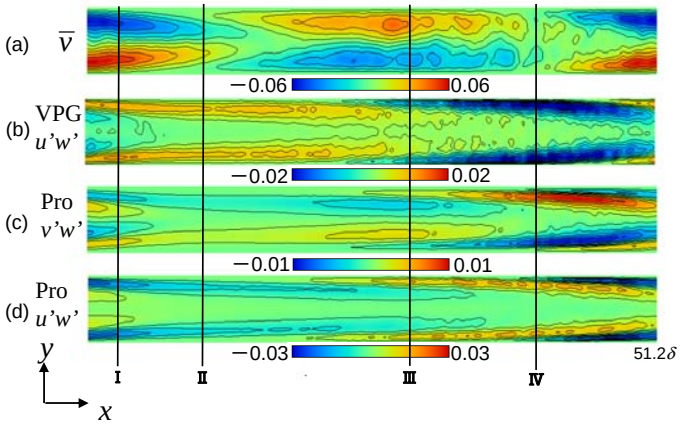

Figure 6. Quasi-mean flow in an (x-y) frame of reference moving with the turbulent stripe: (a) quasi-mean wall-normal velocity, (b) VPG term of budget for Reynolds stress $w'u'$, (c,d) production term of budgets for Reynolds stresses $v'w'$ and $w'u'$.

wall-normal direction. In the area from (I) to (III), the reduction in the turbulent kinetic energy is caused by the local acceleration of the mean flow.

As a result of using ensemble-averaged, a secondary flow with the wall-normal and spanwise components is found to occur, as given in Fig. 3. Therefore, we calculated the budget for Reynolds stresses $v'w'$ and $w'u'$. It can be expected that the turbulent kinetic energy should be transferred between the quasi-laminar region and the turbulent region. Figures 5(c) and 5(d) show the advection terms of the budget for $u'u'$ and $v'v'$. The kinetic energy is found to be transferred back and forth of the turbulent regions: in the vicinity of the wall, the energy is transferred from the upstream to the downstream of the turbulent region, while in the core region, the energy is transferred in the opposite direction. The spatial energy transport will be discussed again later.

Figure 6(a) shows the contour of the quasi-mean velocity in wall-normal direction, and other figures show the contours of the VPG term for $w'u'$ (b) and of the production terms for $v'w'$ (c) and $w'u'$ (d). As seen in Figs 6(b), (c) and (d), the production of the Reynolds stresses as well as their redistribution are significant in the turbulent region (III–IV–I). In Fig. 6(b), it is found that the turbulent energy is exchanged by the VPG term between the turbulent and the quasi-laminar regions. As can be seen from Figs. 6(c) and 6(d), the productions for $v'w'$ and $w'u'$ are significant in the turbulent region.

To discuss statistical characteristics of the quasi-laminar and turbulent regions, a criterion should be determined to distinguish between them. Barkley & Tuckerman [6] distinguished local turbulent regions by integrated turbulent kinetic energy, and they

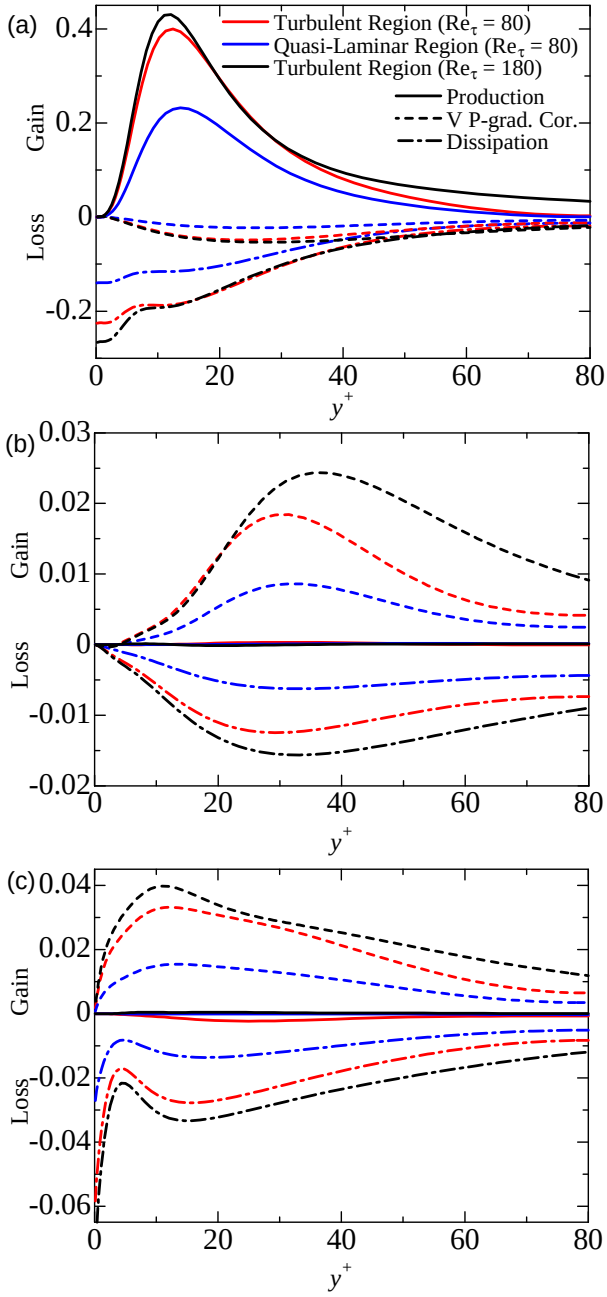

Figure 7. Budget of Reynolds stress divided turbulent region and quasi-laminar region. (a) Reynolds stress $u'u'$, (b) Reynolds stress $v'v'$, (c) Reynolds stress $w'w'$.

confirmed the validity of this criterion. In this study, we employed a similar procedure to yield statistics in the localized turbulent (or quasi-laminar) region. Figures 7(a), (b) and (c) show the budget of Reynolds stress ($\overline{u'u'}$, $\overline{v'v'}$ and $\overline{w'w'}$) averaged in

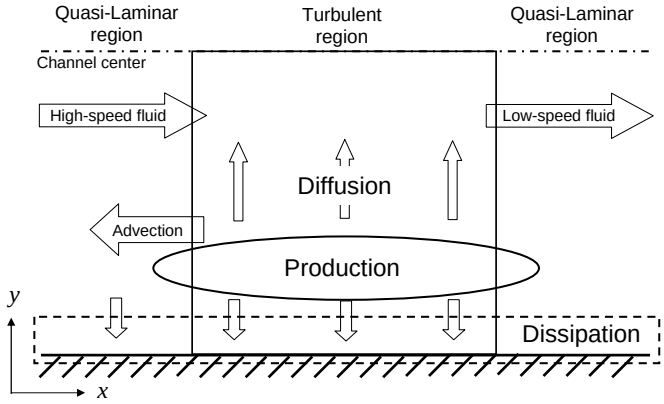

Figure 8. Schematic of the turbulent-energy transport in channel flow.

quasi-laminar or turbulent region. In the figures, the production, dissipation and VPG terms in each Reynolds stress are shown. It can be clearly seen that all the terms for the quasi-laminar region are significantly smaller than those in the turbulent regions, and the peak location of each term tends to shift to the channel center. These behaviors are similar to those by a typical low-Reynolds-number effect, by which the viscous sub-layer should be thickened. The energy balance for the Reynolds stress of $u'u'$ is found to be almost identical between the turbulent region at $Re_\tau = 80$ and the (fully-turbulent) flow field at $Re_\tau = 180$, see Fig. 7(a). In particular, the VPG terms for these two cases are in good agreement. Therefore, it can be conjectured that the turbulent region maintains itself as similar to a flow at higher Reynolds numbers. In Fig. 7(c), the production term is negative value. This result indicates that the turbulent energy is changed to the mean-flow kinetic energy.

Finally, we discuss how the TSS is related to the energy-transport process between the mean flow and the turbulent kinetic energy, and how the large-scale flow structures are related to the exchange of turbulent kinetic energy between the turbulent and quasi-laminar region. Figure 8 shows a schematic of the energy-transport process between the quasi-laminar and turbulent regions. As mentioned previously, the advection velocity of turbulent region can be assumed to be constant over the entire channel and equal to balk mean velocity. In the region away from the wall, especially, at the channel center, the turbulent region moves slower than the quasi-laminar region, and thereby it impinges on a downstream quasi-laminar region. In contrast, near-wall low-speed streaks in the turbulent region are shifted leftward in the figure, where a frame of reference moves with the TSS, and then some fluctuations occurs in the quasi-laminar region.

Figure 9 shows the transport of turbulent energy from the production to dissipation. About 63% of the total turbulent ki-

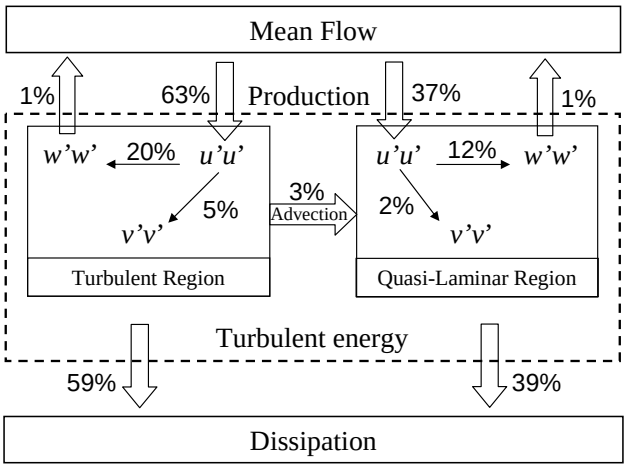

Figure 9. Schematic of the turbulent-energy transport process between quasi-laminar and turbulent regions.

netic energy in the flow field is generated in the turbulent region and the other 37% in the quasi-laminar region. Here, note that the sum of produced turbulent energy from the mean-flow energy is 100%. In the turbulent region, 20% of the $u'u'$ energy is redistributed to $w'w'$, and other 5% is to $v'v'$. It is interesting to note that the energy transferred by the advection term to the quasi-laminar region is only 3%. The turbulent energy in each region is almost dissipated there, but 2% is changed adversely to the mean flow.

CONCLUSIONS

A direct numerical simulation is carried out to investigate turbulent structures in the turbulent plane Poiseuille flow at a very low-Reynolds number in the transitional regime. The flow accompanied by localized quasi-laminar and turbulent regions gave rise to the turbulent-stripe structure. The fluid is visualized as a rheoscopic fluid, in which imaginary flake particles are suspended and by volume rendering. Using this method, quasi-laminar and turbulent regions are adequately distinguished from each other. It is found by conditionally ensemble-averaging that the turbulent region is flanked by the high- and low-speed fluid, which appear on the upstream and downstream sides of the turbulent region, respectively. The spatial outline of the energy transport with emphasis on the turbulent stripe is proposed. The turbulent energy is produced in both the turbulent region and the quasi-laminar region, and the energy transfer between these two regions is found to be small.

ACKNOWLEDGMENT

The present computations were performed with the use of the supercomputing resources at Cyberscience Center Tohoku University. This study was partially supported by the Ministry of Education, Science, Sports and Culture, Grant-in-Aid for Young Scientists (#20860070, FY2008–09) and (#22760136, FY2010).

REFERENCES

[1] T. Tsukahara, Y. Seki, H. Kawamura, and D. Tochio, DNS of turbulent channel flow at very low Reynolds numbers, In: *Proc. of the Forth Int. Symp. on Turbulence and Shear Flow Phenomena*, Williamsburg, USA, Jun. 27–29 (2005), pp. 935–940.

[2] T. Tsukahara, K. Iwamoto, H. Kawamura, and T. Takeda, DNS of Heat Transfer in a Transitional Channel Flow Accompanied by a Turbulent Puff-like Structure, In: *Proc. of the First Int. Symp. on Turbulence, Heat and Mass Transfer*, Dubrovnik, Croatia, Sep. 25–29 (2006), pp. 193–196.

[3] T. Tsukahara, A. Hasobe, Y. Kawaguchi, and H. Kawamura, Study of turbulent puff in transitional channel flow with passive scalar transport, In: *Proc. of the Second Int. Forum on Heat Transfer*, Tokyo, Japan, Sep. 17–19 (2008), p. 28.

[4] T. Tsukahara, Y. Kawaguchi, H. Kawamura, N. Tillmark, and P.H. Alfredsson, Turbulence stripe in transitional channel flow with/without system rotation, In: *Proc. of the Seventh IUTAM Symposium on Laminar-Turbulent Transition*, (eds. P. Schlatter & D.S. Henningson), IUTAM Bookseries, Vol. 18, Springer (2009), pp. 421–426.

[5] H. Abe, H. Kawamura, and Y. Matsuo, Surface heat-flux fluctuations in a turbulent channel flow up to $Re_\tau = 1020$ with $Pr = 0.025$ and 0.71, *Int. J. Heat and Fluid Flow*, 25 (2004), 404–419.

[6] D. Barkley and L.S. Tuckerman, Computational study of turbulent laminar patterns in Couette flow, *Phys. Rev. Lett.*, 94 (2005), 014502.

[7] D. Barkley and L.S. Tuckerman, Mean flow of turbulent-laminar patterns in plane Couette flow, *J. Fluid Mech.*, 576 (2007), 109–137.

[8] Y. Duguet, P. Schlatter, and D.S. Henningson, Formation of turbulent patterns near the onset of transition in plane Couette flow, *J. Fluid Mech.*, 650 (2010), 119–129.

[9] D. Coles, Transition in circular Couette flow, *J. Fluid Mech.*, 21 (1965), 385–425.

[10] C.D. Andereck, S.S. Liu, and H.L. Swinney, Flow regimes in a circular Couette system with independently rotating cylinders, *J. Fluid Mech.*, 164 (1986), 155–183.

[11] K. Fukudome, O. Iida, and Y. Nagano, The turbulent structures of Poiseuille flows at low-Reynolds numbers, In: *Proc. of the Seventh JSME-KSME Thermal and Fluids En-*

gineering Conference, Sapporo, Japan, Oct. 13–16 (2008), K112, (CD-ROM), 4pp.

[12] K. Fukudome, O. Iida, and Y. Nagano, In: *Proc. of the Sixth Int. Symp. on Turbulence and Shear Flow Phenomena*, Seoul, Korea, Jun. 22–24 (2009), pp. 471–476.

[13] W.L. Barth and C.A. Burns, *IEEE Trans. Visualization and Computer Graphics*, 13 (2007), 1751–1758.

[14] S. Hashimoto, A. Hasobe, T. Tsukahara, Y. Kawaguchi, and H. Kawamura, Experimental study on turbulent-stripe structure in transitional channel flow, In: *Proc. of the Sixth Int. Symp. on Trubulence, Heat and Mass Transfer*, Rome, Italy, Sep. 14–18 (2009), pp. 193–196.